

# The Mitochondrial Endonuclease M20 Participates in the Down-Regulation of Mitochondrial DNA in Pollen Cells<sup>1</sup>

Fei Ma,<sup>a,2</sup> Hui Qi,<sup>a,2,3</sup> Yu-Fei Hu,<sup>b</sup> Qian-Ru Jiang,<sup>a</sup> Li-Guang Zhang,<sup>a</sup> Peng Xue,<sup>c</sup> Fu-Quan Yang,<sup>c,d</sup> Rui Wang,<sup>a</sup> Yan Ju,<sup>a,4</sup> Hidenobu Uchida,<sup>a,e</sup> Quan Zhang,<sup>a,5</sup> and Sodmergen<sup>a,5,6</sup>

<sup>a</sup>Key Laboratory of Ministry of Education for Cell Proliferation and Differentiation, College of Life Sciences, Peking University, Beijing 100871, China

<sup>b</sup>College of Life Sciences, South China Agricultural University, Guangzhou 510642, China

<sup>c</sup>Institute of Biophysics, Chinese Academy of Sciences, Beijing 100101, China

<sup>d</sup>University of Chinese Academy of Sciences, Beijing 100049, China

<sup>e</sup>Department of Chemical Biological Sciences, Faculty of Science, Japan Women's University, Tokyo 112-8681, Japan

ORCID IDs: 0000-0003-4392-6930 (Y.-F.H.); 0000-0002-6943-6019 (S.)

Maintaining the appropriate number of mitochondrial DNA (mtDNA) molecules is crucial for supporting mitochondrial metabolism and function in both plant and animal cells. For example, a substantial decrease in mtDNA levels occurs as a key part of pollen development. The molecular mechanisms regulating mtDNA copy number are largely unclear, particularly with regard to those that reduce mtDNA levels. Here, we identified and purified a 20-kD endonuclease, M20, from maize (*Zea mays*) pollen mitochondria. We found M20 to be an His-Asn-His/Asn (H-N-H/N) nuclease that degrades linear and circular DNA in the presence of Mg<sup>2+</sup> or Mn<sup>2+</sup>. Arabidopsis (*Arabidopsis thaliana*) AtM20, which shared high sequence similarity with maize M20, localized to the mitochondria, had a similar H-N-H/N structure, and degraded both linear and circular DNA. *AtM20* transcript levels increased during pollen development, in parallel with a rapid reduction in mtDNA. Clustered regularly interspaced short palindromic repeats (CRISPR)/CRISPR-associated protein 9 genome-editing techniques were used to generate knockout lines of *AtM20* (*atm20*), which exhibited a significant delay in the reduction in mtDNA levels in pollen vegetative cells but normal mtDNA levels in somatic cells. The delayed reduction in pollen mtDNA levels was rescued by the transgenic expression of *AtM20* in *atm20* plants. This study thus uncovers an endonucleolytic DNase in plant mitochondria and its crucial role in reducing mtDNA levels, pointing to the complex mechanism regulating mtDNA levels in plants.

Mitochondria are key organelles that generate energy (ATP) for eukaryotic cells and mediate cellular processes such as apoptosis, calcium signaling, and reactive oxygen species (ROS) homeostasis (Attardi and Schatz, 1988; Wallace, 2008). Mitochondria, which

were originally derived from bacterial endosymbionts, contain small DNA molecules termed mitochondrial genomes that support their metabolism and function (oxidative phosphorylation). These genomes are small; for example, mitochondrial genomes in human are only 16.6 kb in length, encoding 22 transfer RNAs and 15 polypeptides (Wallace, 2008). However, numerous clinical symptoms, such as nerve and muscle dysfunction, reduced fertility, diabetes, cancer, aging, Parkinson's disease, and many other diseases, are associated with mutations in the human mitochondrial genome (for reviews, see Wallace and Murdock, 1999; Dimauro and Davidzon, 2005; Schapira, 2012). Plant mitochondrial genomes are usually larger than those in human. For example, Arabidopsis (*Arabidopsis thaliana*) contains a 372-kb mitochondrial genome encoding 22 transfer RNAs and 36 polypeptides (Klein et al., 1994). Since precision medicine is not performed in plants, little is known about mitochondrial diseases in plants. However, a classical agronomic trait that is widely used in crop production, cytoplasmic male sterility, could be considered a plant mitochondrial disease, albeit one with important applications for production of hybrid seed. Abnormal recombination in the mitochondrial genome underlies abnormalities in male fertility (Wang et al., 2006; Luo et al., 2013). Clearly, the

<sup>1</sup>This work was supported by the National Basic Research Program of China (grant 2013CB126905).

<sup>2</sup>These authors contributed equally to this work.

<sup>3</sup>Current address: Max Plank Institute for Heart and Lung Research, Department of Cardiac Development and Remodeling, 61231 Bad Nauheim, Germany

<sup>4</sup>Current address: Department of Botany and Plant Pathology, Purdue University, Lilly Hall of Life Sciences, 915 W. State St. West Lafayette, Indiana 47907

<sup>5</sup>Senior authors.

<sup>6</sup>Author for contact: sodmergn@pku.edu.cn.

The author responsible for distribution of materials integral to the findings presented in this article in accordance with the policy described in the Instructions for Authors ([www.plantphysiol.org](http://www.plantphysiol.org)) is: Sodmergen (sodmergn@pku.edu.cn).

F.M. and H.Q. designed the study, performed the experiments, analyzed the data, and prepared this article; Y.-F.H., Q.-R.J., L.-G.Z., P.X., F.-Q.Y., R.W., Y.J., and H.U. performed some experiments; Q.Z. conducted the experiments; S. conceived the project and revised the article.

[www.plantphysiol.org/cgi/doi/10.1104/pp.18.00754](http://www.plantphysiol.org/cgi/doi/10.1104/pp.18.00754)

correct composition and expression of mitochondrial genes are essential for proper cellular functioning in eukaryotes.

Another mitochondrial factor that is almost equally important for the functioning of eukaryotic cells is the copy number of mitochondrial genomes per cell. In animals, cells in a given tissue contain a constant amount of mitochondrial DNA (mtDNA), which usually ranges from 1,000 to 10,000 copies per cell, depending on the tissue or cell type (Masuyama et al., 2005; Xie et al., 2015). Changes in the copy number of mtDNA per cell, including either an increase or decrease, cause dysfunction in the mitochondria and result in the diseases described above (for reviews, see Higuchi, 2007; Clay Montier et al., 2009). A proper and stable amount of mtDNA is therefore required to ensure cellular functioning.

Plant cells possess relatively low levels of mtDNA, with up to 300 to 400 copies per cell in root tips and only 40 to 140 copies per cell in other tissues (Preuten et al., 2010). Strikingly, through direct observation, we previously determined that one-third of the mitochondria in *Arabidopsis* leaf cells contain a partial genome, comprising approximately 100 kb of mtDNA, while over two-thirds of mitochondria contain absolutely no DNA (Wang et al., 2010). This finding is in contrast to our knowledge about animal cells, in which each mitochondrion is thought to contain at least one copy of mtDNA; each human, rabbit, rat, and mouse mitochondrion was shown to contain an average of  $2.6 \pm 0.3$  copies of mtDNA (Robin and Wong, 1988). Given that an *Arabidopsis* leaf cell contains approximately 670 mitochondria (Sheahan et al., 2005), it appears that approximately 10 mitochondria share one complete genome in a cell. Plant mitochondria undergo frequent and coupled fusions and divisions, which explains how mitochondria share this information (Arimura et al., 2004; Arimura, 2018). The low copy number of mtDNA in plant mitochondria has also been observed in egg and pollen cells, a phenomenon termed “the genomic insufficiency of plant mitochondria” (Wang et al., 2010; Cai et al., 2015). Interestingly, although there are great differences in mtDNA copy number between plant and animal cells, changes in copy number in both types of organisms result in mitochondrial defects. Increases in mtDNA copy number in *Arabidopsis* pollen vegetative cells were recently shown to cause reduced ATP production, the overproduction of ROS, and inhibited pollen tube growth (Cai et al., 2015).

It is clear that maintaining the proper copy number of mtDNA is essential for both plant and animal cells. However, the mechanism that regulates mtDNA copy number is largely unknown. The turnover of mtDNA occurs very rapidly: the half-life of mtDNA in rat is several days or fewer (Gross et al., 1969; Kai et al., 2006), and only 24 h are required for the complete turnover of mtDNA in mung bean (*Vigna radiata*; Dai et al., 2005). These findings imply that both plant and animal cells undergo rapid mtDNA replication at a rate equivalent to that of turnover to stabilize copy number. In fact, rapid and continuous mtDNA replication indeed

occurs in animal mitochondria independent of the cell cycle (Bogenhagen and Clayton, 1977; Magnusson et al., 2003). It is thus thought that the regulation of mtDNA copy number in cells must occur in a highly dynamic, well-balanced manner in which up-regulation (replication) is triggered when the copy number is low and down-regulation (turnover) is triggered when the copy number is high (Clay Montier et al., 2009). This regulatory model is logical and fact based, although several key points of the model, such as the molecular mechanism that monitors cellular mtDNA copy number and the regulatory pathways that trigger replication and turnover, remain to be elucidated.

According to the current hypothesis, both the up- and down-regulation of mtDNA play equally important roles in maintaining the proper mtDNA copy number in a cell. A group of replication-related factors are known to be involved in mtDNA replication in animals, such as DNA polymerase (Sharief et al., 1999), RNA polymerase (Wanrooij et al., 2008), mtDNA helicase (Liu et al., 2009), and mitochondrial single-stranded DNA binding protein (Maier et al., 2001). Similarly, mtDNA polymerases IA and IB are involved in mtDNA replication in *Arabidopsis* (Parent et al., 2011). Another group of protein factors that bind to mtDNA, including MITOCHONDRIAL TRANSCRIPTION FACTOR A and WHIRLY2, are thought to protect mtDNA from degradation in human (Alam et al., 2003) and *Arabidopsis* (Cai et al., 2015), respectively. However, although turnover is another component required for maintaining mtDNA at the proper levels, little is known about the molecules that are directly responsible for mtDNA down-regulation. The only such molecule identified to date is DEFECTIVE IN POLLEN ORGANELLE DNA DEGRADATION1 (DPD1), an exonuclease found in plant mitochondria and plastids (Matsushima et al., 2011; Shen et al., 2015; Sakamoto and Takami, 2018). The down-regulation of mtDNA copy number is significantly impaired in the pollen cells of *dpd1* mutants (Matsushima et al., 2011; Shen et al., 2015). Moreover, given that the majority of mtDNA exists in circular form (Kolodner and Tewari, 1972; Kool et al., 1985; Satoh et al., 1993; Kayal et al., 2012), the complete degradation of mtDNA must require an additional mitochondrial endonuclease that has yet to be identified in plants.

In this study, we identified a DNase, which we termed M20, from maize (*Zea mays*) pollen mitochondria and purified it using biochemical approaches. We found that M20 and AtM20, the homologous protein in *Arabidopsis*, share the typical molecular features of His-Asn-His/Asn (H-N-H/N) nucleases and that both had endonuclease activity *in vitro*. Using the clustered regularly interspaced short palindromic repeats (CRISPR)/CRISPR-associated protein9 (Cas9) knock-out technique, we performed intensive analysis of AtM20 and showed the participation of this mitochondrial endonuclease in the reduction of mtDNA levels in pollen cells. Our findings uncover the requirement for multiple DNases in mtDNA degradation, highlighting

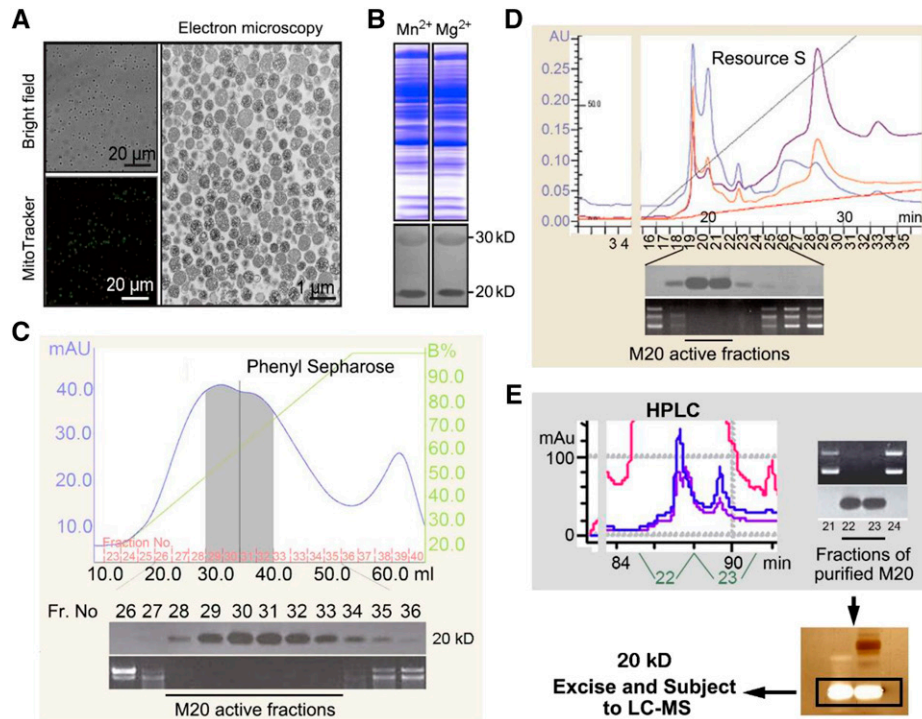


**Figure 1.** Purification and identification of M20 from maize pollen mitochondria. A, Quality monitoring of purified mitochondria from maize pollen by bright field (top left), fluorescence (bottom left, the same field stained with MitoTracker Green), and transmission electron microscopy (right). B, Total mitochondrial proteins after SDS-PAGE (top) and in-gel activities of mitochondrial nucleases M20 and M30 in the presence of  $Mn^{2+}$  and  $Mg^{2+}$  (bottom). C to E, Purification of M20 by hydrophobic chromatography (C), cation-exchange chromatography (D), and HPLC (E). The nucleolytic activity of M20 was monitored via both in-gel and plasmid (pUC18) digestion assays. Single M20 bands (white and transparent in a silver-stained SDS-PAGE gel) were excised and subjected to LC-MS analysis.

the complexity of the molecular mechanisms underlying mtDNA homeostasis in plant cells.

## RESULTS

### Purification of M20 from Pollen Mitochondria

mtDNA undergoes rapid, massive degradation during pollen development (Sodmergen and Suzuki, 1992; Nagata et al., 1999; Wang et al., 2010), providing us with an appropriate model for studying mtDNA down-regulation. We collected premature, fresh pollen grains from maize and purified pollen mitochondria via a step-by-step procedure (Supplemental Fig. S1). We obtained pollen mitochondria with almost no contamination after a secondary centrifugation through Suc gradients (Fig. 1A). We loaded a lysate of purified mitochondria onto a sodium dodecyl sulfate-polyacrylamide gel electrophoresis (SDS-PAGE) gel pre-embedded with DNA to identify protein molecules with DNA hydrolytic activity (in-gel assay; Rosenthal and Lacks, 1977). We identified two proteins with  $M_r$ s of 20 kD and 30 kD, namely M20 and M30, exhibiting nucleolytic activity in the presence of  $Mn^{2+}$  or  $Mg^{2+}$

(Fig. 1B). We focused our analysis on M20 due to its water solubility and robust in-gel activity.

We purified M20 using two different methods. For both methods, we performed prepurification by treating the supernatant of a mitochondrial lysate with ammonium sulfate to salt out the active components (Supplemental Fig. S1) and subjected the components to hydrophobic interaction chromatography on a phenyl-Sepharose column after dialysis (Fig. 1C).

For further purification, we performed ion-exchange chromatography (Fig. 1D), followed by high-performance liquid chromatography (HPLC; Fig. 1E) for the first method and gel filtration followed by heat precipitation for the second method (Supplemental Fig. S1). Using an in-gel assay with silver staining, we confirmed the presence of clear bands with M20 activity in both gels (Fig. 1E; Supplemental Fig. S1). Finally, we performed liquid chromatography-mass spectrometry (LC-MS) to analyze the gel contents (activity bands). The results from both gels yielded identical peptide information, i.e. M20 corresponds to the product of the maize gene ACG45136.1. These results indicate that we successfully identified M20, a soluble mitochondrial DNase from maize with heat stability.

## M20 Is an H-N-H(N) Endonuclease

Bioinformatic analysis involving searches against the National Center for Biotechnology Information (NCBI) *Zea mays* protein database revealed that ACG45136.1 encodes a putative endonuclease/nucleic acid binding protein with a molecular mass of 20 kD (Supplemental Fig. S2). A comparison with the nucleolytic molecules identified to date revealed that M20 shares an H-N-H/N domain, i.e. a nonconsecutive His-Asn-His/Asn motif, that forms a conservative  $\beta$ - $\beta$ - $\alpha$  structure found in a group of endonucleases identified in bacterial, phage, and animal cells (Fig. 2A). The molecular characteristics of M20 are not unexpected, since the  $\beta$ - $\beta$ - $\alpha$  structure is essential for the binding of bivalent cations and is crucial for nuclease catalytic activity (Mehta et al., 2004). To investigate the evolutionary conservation of M20 in plants, we performed further BLAST searches of M20 homologs using the entire amino acid sequence of M20 as a query against the GenBank database (<http://www.ncbi.nlm.nih.gov/genbank/>). The results revealed M20 homologs in plants ranging from a moss (*Physcomitrella patens*) to a fern (*Selaginella moellendorffii*) and most spermatophytes (Supplemental Fig. S2), suggesting that this molecule is highly conserved in plants.

An analysis of the Arabidopsis genome showed that the protein encoded by At1g18680 shares high similarity (63%) with M20 and also contains an H-N-H/N domain (Supplemental Fig. S2). We designated this putative protein AtM20. Since the H-N-H/N domain is a molecular feature of endonucleases (Mehta et al., 2004), we reasoned that M20, as well as AtM20, might exhibit endonuclease activity to hydrolyze DNA. This notion was verified using an *in vitro* digestion assay. Both purified M20 and the recombinant products, M20-GST and AtM20-His, hydrolyzed circular plasmid DNA (Fig. 2B). In addition, point mutations in the H-N-H/N domain blocked the hydrolytic activity of M20-GFP and AtM20-GFP (Fig. 2, C and D). These results indicate that M20, together with its Arabidopsis homolog AtM20, are endonucleases and that the H-N-H/N domains within these molecules are indispensable for their hydrolytic activity. The similarities between M20 and AtM20 in terms of amino acid sequence,  $M_r$ , conserved H-N-H/N domain, and *in vitro* endonuclease features suggest that these molecules play conserved roles in maize and Arabidopsis.

## AtM20 Localizes to Pollen Mitochondria

To investigate the functions of these endonuclease molecules and their conservation between maize and Arabidopsis, we performed GUS reporter activity analysis and reverse transcription quantitative PCR (RT-qPCR) to examine the expression patterns of AtM20 in different tissues. We detected GUS signals in pollen (Fig. 3A), with the highest transcript accumulation in tricellular pollen (TCP) (Fig. 3B). We did not observe GUS signals in other tissues, although RT-qPCR revealed low levels of *AtM20* transcript in roots, stems, leaves,

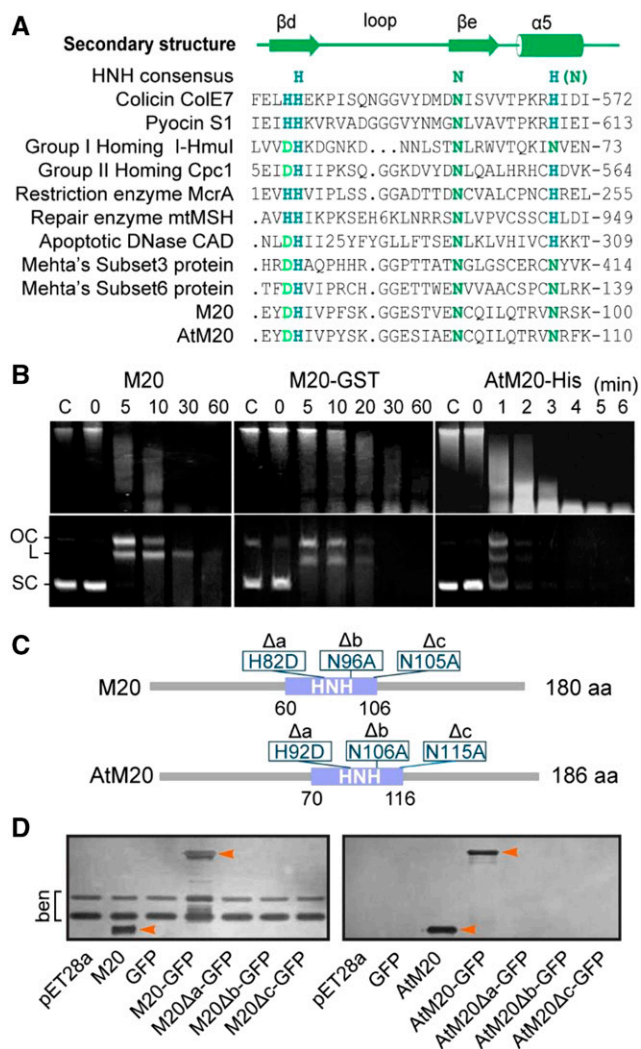


**Figure 2.** M20 and AtM20 are H-N-H(N) nucleases with endonucleolytic activity *in vitro*. **A**, Partial sequence alignment of M20 with representative endonuclease proteins with H-N-H(N) domains. Conserved residues comprising the H-N-H(N) domain are shown in different shades of green. The secondary structure derived from the crystal structure of nuclease-ColE7 is shown above the alignment. Numbers indicate omitted amino acids. AtM20, a highly similar molecule in Arabidopsis, shares very close sequence features with M20. **B**, Catalytic features of purified M20, recombinant M20-GST, and AtM20-His proteins. Salmon sperm DNA (top) and the pUC18 plasmid (bottom) were used as substrates. **C**, Control; OC, open-circular DNA; L, linear DNA; SC, supercoiled DNA. **C**, Schematic representation of point mutations in M20 and AtM20. The positions of the point mutations and amino acid conversions are shown in blue boxes. **D**, In-gel assays showing the nuclease activity of M20-GFP and AtM20-GFP fusion proteins. Cell lysates of *E. coli* expressing recombinant M20-GFP, AtM20-GFP, and genes with point mutations were analyzed by in-gel assays. A recombinant line expressing M20 was used as the positive control, and recombinant lines expressing the empty pET28a vector and GFP were used as negative controls. Arrowheads indicate the activity bands of M20, M20-GFP, AtM20, and AtM20-GFP; ben, bacterial endogenous nucleases. AtM20 and AtM20-GFP showed much higher in-gel activity than bacterial endogenous nucleases (ben), which had not yet emerged after the optimal incubation time.

and siliques (Fig. 3B). These results indicate that *AtM20* is expressed ubiquitously but at low levels, with the highest levels detected in pollen; these results are in agreement with microarray data from the Arabidopsis eFP Browser database ([http://bar.utoronto.ca/efp\\_arabidopsis/cgi-bin/efpWeb.cgi](http://bar.utoronto.ca/efp_arabidopsis/cgi-bin/efpWeb.cgi); Supplemental Fig. S3). During pollen development, *AtM20* transcript levels began to increase in bicellular pollen (BCP), reached a peak in TCP, and then decreased sharply in mature pollen grains (Fig. 3B). Notably, this expression pattern fits the pattern of mtDNA degradation during pollen development (Sodmergen and Suzuki, 1992; Nagata et al., 1999; Wang et al., 2010), pointing to a possible relationship between *AtM20* and the down-regulation of mtDNA in pollen.

We then examined whether *AtM20* localizes to mitochondria by performing transient expression analysis of an *AtM20*-GFP fusion protein in *Nicotiana benthamiana* leaf cells. We detected a clear merging of GFP fluorescent signals with those of mitochondria (Fig. 3C), indicating that *AtM20* is a mitochondrial protein (nuclease) that is likely involved in pollen mtDNA degradation. To confirm the higher expression level of *AtM20* in pollen (as indicated at the RNA level via GUS reporter and RT-qPCR analyses; Fig. 3, A and B), we constructed transgenic plants harboring *AtM20*-GFP driven by its native promoter (*AtM20<sub>pro</sub>*-*AtM20*-GFP). The construct was transformed into LAT52<sub>pro</sub>-Dips-RFP plants, an independent transgenic line in which pollen mitochondria exhibit red fluorescent protein fluorescence (Matsushima et al., 2011). In the pollen cells of these transgenic lines, we again observed the colocalization of *AtM20*-GFP with fluorescent signals from mitochondria (Supplemental Fig. S4). Notably, however, the fluorescent signals from *AtM20*-GFP were very weak and had to be captured using enhanced exposure. This is a common characteristic of DNases, which are present at very low abundance (discussed below). Indeed, fluorescent signals from *AtM20*-GFP were undetectable in leaf cells using the same exposure conditions (Supplemental Fig. S4). These results are in good agreement with the transcription pattern of *AtM20*, suggesting it is a mitochondrial nuclease that may function in mtDNA degradation in pollen.

#### *AtM20* Participates in mtDNA Degradation in Pollen

We used CRISPR/Cas9 technology (Feng et al., 2013, 2014; Miao et al., 2013) to specifically knock out the *AtM20* gene in Arabidopsis, since all of the transfer DNA (T-DNA) insertion lines examined, including five from ABRC ([www.arabidopsis.org/servlets/order](http://www.arabidopsis.org/servlets/order)) and one from GABI-KAT ([www.gabi-kat.de/](http://www.gabi-kat.de/)), were unusable; *AtM20* expression was not disrupted in any of these lines, as revealed by RT-qPCR (Supplemental Fig. S5). We designed three *AtM20*-specific spacers (single guided RNA1-3 [sgRNA1-3]) for the expression of guide RNAs driven by the *AtU6-26* promoter (Fig. 4A; Supplemental Fig. S6). Transformations using whole vectors containing sgRNA cassettes and additional

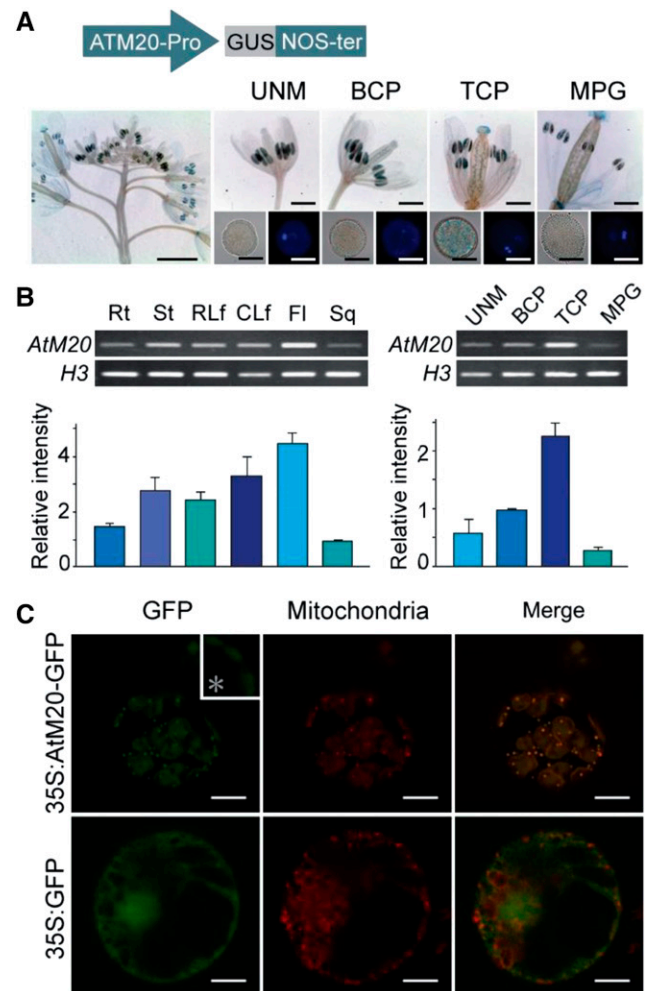


**Figure 3.** *AtM20* has a higher expression in pollen and localizes to mitochondria. **A**, *AtM20* promoter-GUS reporter analysis. The pollen grains were stained with DAPI (4',6-diamino-phenylindole) to clarify the developmental stages. UNM, Uninucleate microspore; BCP, bicellular pollen; TCP, tricellular pollen; MPG, mature pollen grain. The bar for the inflorescence GUS image is 5 mm; bars for flower GUS images are 1 mm, and bars for all pollen images are 5  $\mu$ m. **B**, RT-PCR analysis of *AtM20* transcript levels in different tissues and pollen cells. The histone variant *H3* was used as the control. Rt, Root; St, stem; Rlf, rosette leaf; CLf, cauline leaf; Fl, flower; Sq, silique. Histograms summarize the results of independent analyses of three biological replicates. Error bars represent the SD. **C**, *AtM20* colocalizes with mitochondria in transiently transformed *N. benthamiana* protoplasts. The cells were transformed with 35S<sub>pro</sub>-*AtM20*-GFP and stained with MitoTracker Red. 35S<sub>pro</sub>-GFP-transformed cells were used as the negative control. \*, a reference picture showing signals of chlorophyll autofluorescence captured from a Col-0 protoplast with the same exposure conditions. Bars, 10  $\mu$ m.

*Cas9* genes driven by the *Cauliflower mosaic virus* (CaMV) 35S promoter (Fig. 4A) yielded a group of T1 transgenic plants with various mutations in *AtM20* (Supplemental Fig. S6). Most mutations involved one or several nucleotide deletions or insertions, in accordance with previous reports (Feng et al., 2013, 2014). Through self-crosses, we identified a homozygous mutant line with a 4-bp deletion (termed d4 mutation)

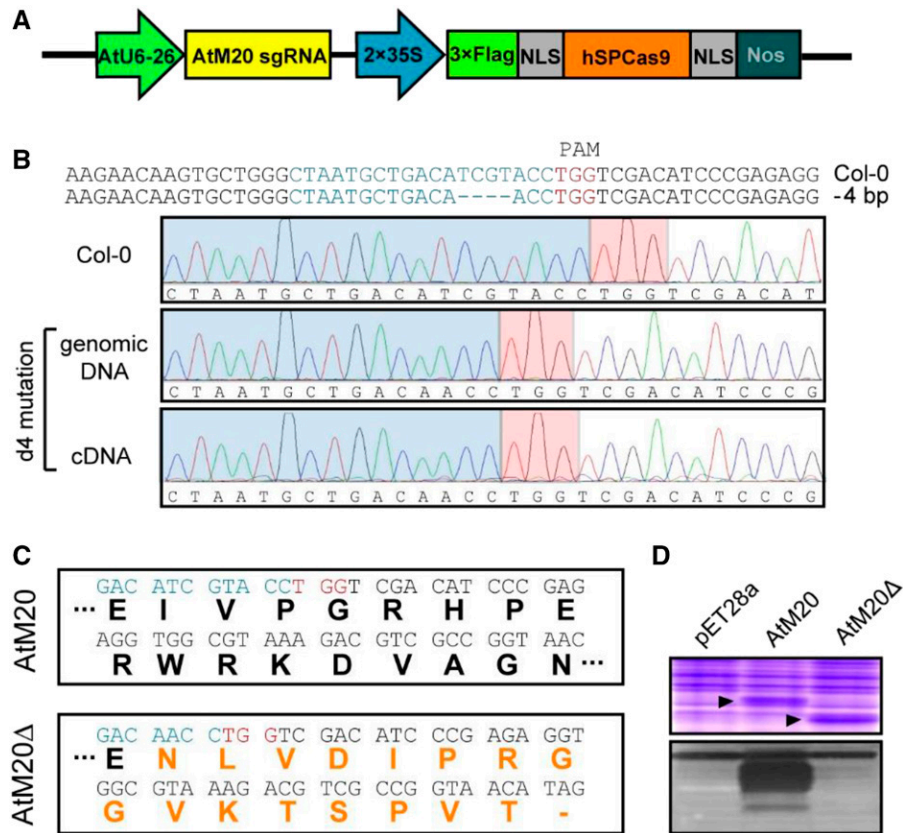


**Figure 4.** Generation of the *atm20* mutant using CRISPR/Cas9 technology. **A**, Schematic diagram of the CRISPR construct containing a Cas9 expression cassette driven by an enhanced CaMV 35S promoter and an sgRNA controlled by the AtU6-26 promoter. **B**, A 4-bp deletion was detected in genomic DNA and cDNA of a T1 transformant (d4 mutation). The target sequence is shaded in blue, and the (PCI/PINT associated module) PAM domain is shaded in red. **C**, The 4-bp deletion within AtM20 and may lead to early translational termination. **D**, A smaller product (AtM20Δ) of AtM20 due to base deletion and early termination was detected in plants with the d4 mutation (top), and the mutation inactivates its nucleolytic activity in vitro (bottom). Arrowheads indicate the molecular products of AtM20 and AtM20Δ.

in the first exon of *AtM20* (Fig. 4B). Sequence analysis of the d4 mutation revealed the occurrence of a frame shift (Fig. 4C) resulting in the loss of the H-N-H(N) structure and a premature stop codon resulting in early translational termination. This mutation was verified by the disappearance of the in-gel activity of the product of the d4 mutation (AtM20Δ), as well as a band shift (Fig. 4D). Therefore, we succeeded in obtaining a genetic line with functional knockout of *AtM20*; we designated the d4 mutant *atm20*.

Using homozygous *atm20* plants, we examined the phenotypes induced by the *AtM20* knockout mutation. We observed a distinct delay in mtDNA down-regulation during pollen development in the mutant. With developmental progression roughly divided into the uninucleate microspore, BCP, and TCP stages (Fig. 5A), the down-regulation occurred during the BCP stage in wild-type Arabidopsis (Col-0), resulting in undetectable fluorescent signals from mtDNA in TCP cells (Fig. 5B). This phenomenon is commonly observed in pollen cells, representing the necessary down-regulation

of mtDNA during pollen development (Sodmergen and Suzuki, 1992; Nagata et al., 1999; Wang et al., 2010; Matsushima et al., 2011). In *atm20* plants, however, the fluorescent signals that are usually detected in BCP cells remained distinct in early TCP cells (Fig. 5B), an unusual observation suggesting that the down-regulation of mtDNA might be impeded in pollen cells. We failed to detect these fluorescent signals in late TCP cells (Fig. 5B), indicating that the down-regulation of mtDNA proceeded at a markedly slower pace in mutant plants lacking AtM20 compared to the wild type. Analysis via qPCR revealed relatively high levels of mtDNA in early TCP cells of the *atm20* mutant (Fig. 5, C and D), confirming the impeded down-regulation of mtDNA in the mutant. Thus, the preservation of mtDNA in early TCP cells is a clear outcome of *AtM20* knockout, which we observed repeatedly in CRISPR/Cas9 mutant lines other than *atm20* (the d4 mutant; Supplemental Fig. S7).

To evaluate the degree of impedance of the down-regulation of mtDNA in the absence of AtM20, we performed quantitative analysis of mtDNA using a

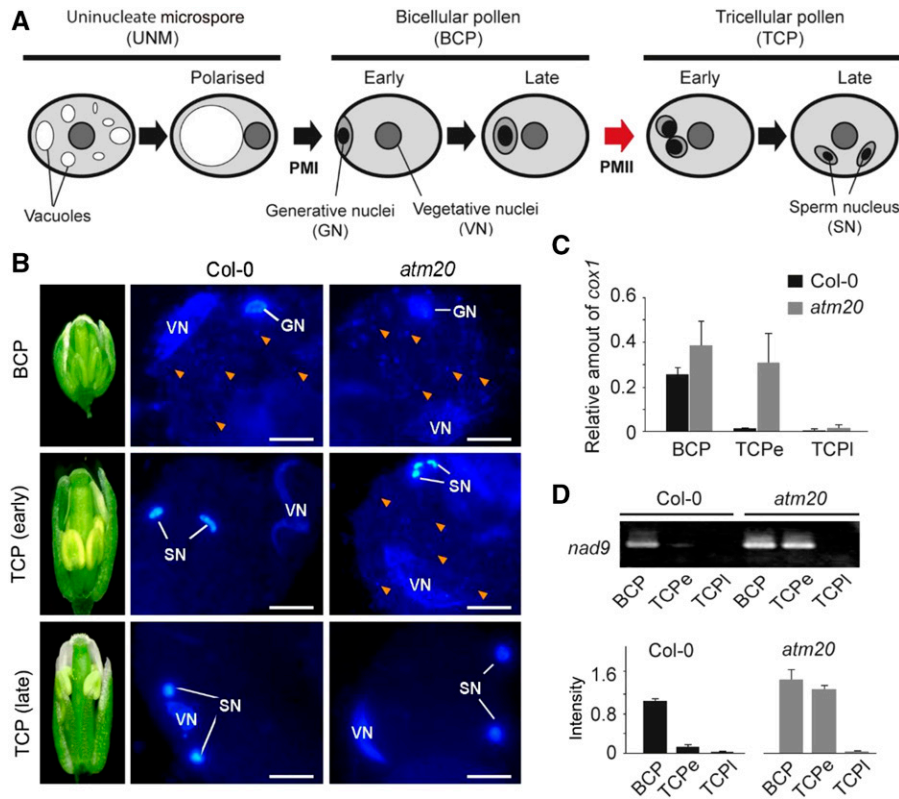


**Figure 5.** Degradation of mitochondrial DNA in pollen vegetative cells is delayed in the *atm20* mutant. A, Schematic diagram of pollen development in Arabidopsis. Red arrow indicates the stage of mtDNA degradation. PMI, Pollen mitosis I; PMII, pollen mitosis II. B, Pollen cells of Col-0 and *atm20* plants observed via DAPI staining. Arrowheads indicate fluorescent signals from organelle DNA (including mtDNA and plastid DNA). Bars, 10  $\mu$ m. C, Relative mtDNA levels analyzed with the mitochondrial *cox1* gene via qPCR. TCPe, Early TCP; TCPi, late TCP. Error bars represent the *sd* ( $n = 3$ ). D, Relative mtDNA levels analyzed with the mitochondrial *nad9* gene via PCR. Histograms summarize the results of independent analyses. Error bars represent the *sd* ( $n = 3$ ).

single-cell-based competitive PCR method to determine the copy number of mtDNA per pollen grain (Wang et al., 2010). In Col-0, early BCP, early TCP, and late TCP grains contained an average of  $131.3 \pm 13.1$ ,  $16.7 \pm 3.5$ , and  $11.3 \pm 1.5$  copies of mtDNA, respectively, whereas in the *atm20* mutant, early BCP, early TCP, and late TCP grains contained an average of  $144.7 \pm 6.1$ ,  $83.7 \pm 12.9$ , and  $17.0 \pm 1.0$  copies per pollen grain, respectively (Supplemental Fig. S8). These values point to the quantitative difference in the progression of mtDNA degradation between Col-0 and *atm20* pollen. Therefore, approximately 90% of mtDNA ( $[131.3 - 11.3]/131.3$ ) was degraded during Col-0 pollen development, with 87% degradation ( $[131.3 - 16.7]/131.3$ ) occurring in BCP cells. In *AtM20* knockout plants, however, a total of 88% of mtDNA ( $[144.7 - 17.0]/144.7$ ) was degraded during pollen development, with 42% degradation occurring in BCP cells ( $[144.7 - 83.7]/144.7$ ) and 46% occurring in TCP cells ( $[83.7 - 17.0]/144.7$ ). Therefore, the absence of *AtM20* in pollen mitochondria led to delayed mtDNA degradation, indicating that *AtM20* participates in the down-regulation of mtDNA in pollen. A complementary experiment showing that transformation

of the *atm20* mutant with the *AtM20* coding sequence rescued the impaired down-regulation of mtDNA (Supplemental Fig. S9) supported this conclusion.

#### Plants Lacking *AtM20* Exhibit Normal Somatic Growth and Reproduction

As indicated above, we detected *AtM20* transcripts in leaves, roots, stems, and siliques (Fig. 3B), although the transcript levels were much lower than that in pollen. This finding suggests that *AtM20* might function in these somatic cells. After careful examination of *atm20* plants, however, we did not identify any alterations in vegetative growth or reproduction. Plant and seed development and morphology were normal in the mutant (Supplemental Fig. S10). We did not detect abnormalities in reproductive growth, including flower and pollen morphology (Fig. 6, A and B), pollen viability and germination (Fig. 6, B to F), pollen tube growth (Fig. 6G), or seed development (Fig. 6H). In addition, we quantified the relative levels of mt- and plastid DNA in leaf cells of Col-0 and *atm20* plants. Again, no significant differences were detected between the lines

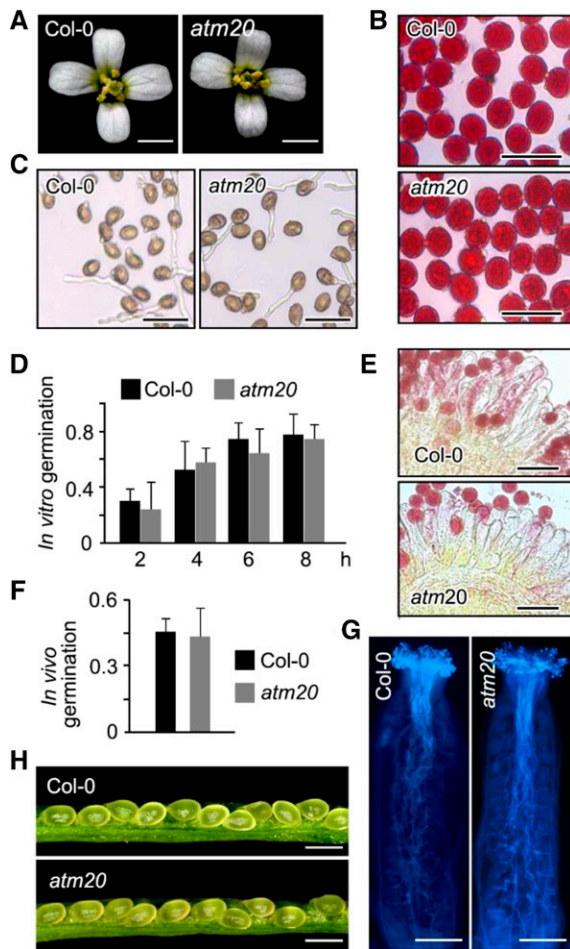


**Figure 6.** Normal reproductive growth and pollen germination in the *atm20* mutant. A, Single flowers from Col-0 and *atm20* plants. Bars, 1 mm. B, Pollen grains from Col-0 and *atm20* plants stained with Alexander solution. Bars, 50  $\mu$ m. C, Col-0 and *atm20* pollen germinated in vitro. Bars, 50  $\mu$ m. D, Pollen germination in vitro. Error bars represent the SD ( $n = 3$ ). E, Col-0 and *atm20* pollen germinated in vivo. Bars, 50  $\mu$ m. F, Pollen germination in vivo. Error bars represent the SD ( $n = 3$ ). G, Pollen tube growth in vivo. Bars, 1 mm. H, Immature Col-0 and *atm20* seeds. Bars, 5 mm.

(Supplemental Fig. S11). These results suggest that the function of AtM20 in somatic cells is not as crucial as that in pollen.

The degradation of mtDNA during pollen development is crucial for normal respiration in pollen. The presence of high levels of mtDNA (approximately 130 copies/TCP) induced by blocking its degradation resulted in reduced male competence (Cai et al., 2015). In the current study, we found that late TCP cells with knockout of *AtM20* had  $17.0 \pm 1.0$  copies of mtDNA (Supplemental Fig. S8), which is significantly higher than the  $11.3 \pm 1.5$  copies detected in Col-0 TCP ( $P < 0.05$ ). To determine whether this higher mtDNA copy number affects male competence in the mutant, we performed reciprocal crosses between Col-0 and heterozygous *atm20* plants. The transmission efficiency

of *atm20* through male or female gametes was not significantly reduced (Supplemental Table S1). These results indicate that although knockout of *AtM20* leads to a significant increase in mtDNA levels in TCP, these increased levels do not appear to affect pollen tube growth or fertilization.

## DISCUSSION

Many important biological processes, such as programmed cell death, DNA repair, gene transmission and organ or cell senescence require the participation of DNase to cleave or degrade DNA molecules. We recently searched the Arabidopsis genome using *DNase* as a query and detected more than 50 open reading frames that are predicted to encode proteins with putative DNase activity (<http://www.arabidopsis.org/index.jsp>). This finding indicates that plants contain a wide variety of DNase molecules. An earlier study using an in-gel assay detected 13 independent DNase molecules from rice (*Oryza sativa*) leaves (Sodmergen et al., 1991), pointing to the complexity of the molecular backgrounds and functions of plant DNases. Due to the importance of DNA hydrolytic activity for numerous biological processes in plants, many studies have focused on identifying specific DNase molecules in particular plant cells, showing that they participate in plant defense responses (Mittler and Lam, 1995), leaf senescence (Canetti et al., 2002), flower and embryo development (Lombardi et al., 2007; Gu et al., 2011), xylem formation (Chen et al., 2012), and other processes (see Sakamoto and Takami, 2014, for review). However, in most studies performed to date, DNase molecules were identified indirectly based on in-gel activity, and there is little evidence that these molecules cleave or degrade DNA in vivo (Sakamoto and Takami, 2014). This can at least be partially attributed to a common molecular characteristic of DNases, namely, their very low abundance in cells despite their sufficiently high activity, impeding the direct purification and characterization of these molecules. In this study, through repeated purification based on the molecular features of DNases, we succeeded in obtaining the minimal amount of purified M20 (lower than the limit of silver staining, presumably 1 ng; Fig. 1E; Supplemental Fig. S1) required for LC-MS analysis from more than 10 kg of fresh maize pollen. Due to the difficulty in directly identifying DNases, we adopted different purification methods, verifying the successful identification of M20.

The very low abundance of DNase impedes the study of cellular localization, as well. Our result showed the existence of *AtM20* transcripts in root, leaf, and stem cells (Fig. 3B), agreeing with the microarray data showing constitutive expression of the gene in Arabidopsis (Supplemental Fig. S3). The fluorescence signals of *AtM20*-GFP, however, were undetectable from the cells except for in pollen (Supplemental Fig. S4). We believe

that such conflicts may be a normal condition in the study of DNase, a protein factor with cellular abundance as low as near the limitation of fluorescence detection. The subcellular localization of AtM20 is a similar case. Our result confirmed the localization within mitochondria (Fig. 3C; Supplemental Fig. S4). This accordingly could not exclude the possibility for a dual-localization of AtM20 in another DNA-containing organelle, plastids, although knockout of *AtM20* does not affect the degradation of plastid DNA during pollen development (Supplemental Fig. S12). In fact, prediction programs suggest both mitochondria (Nair and Rost, 2005) and plastids (Emanuelsson et al., 2000) as potential targets for AtM20.

The regulation of mtDNA levels is another important biological process that requires the participation of DNase. Unlike the nuclear genome, in which stable levels of chromosomes are usually maintained in differentiated cells, mitochondrial genome levels are regulated via the dynamic balance between continuous replication and turnover (Clay Montier et al., 2009). Although mitochondrial DNase is thought to be indispensable for mtDNA turnover and down-regulation, little is known about this molecule in plants or animals. To the best of our knowledge, DPD1 is the first mitochondrial DNase that was shown to degrade mtDNA in vivo in *Arabidopsis*. DPD1 is a plastid- and mitochondrial-localized exonuclease associated with the down-regulation of plastid and mtDNA in pollen to the minimum required levels (Matsushima et al., 2011; Shen et al., 2015), providing the first direct evidence for the participation of DNase in the regulation of mtDNA levels. In flowering plants including *Arabidopsis*, mtDNA is significantly down-regulated during pollen development to approximately 10 copies (the minimum required level) per pollen grain (Wang et al., 2010). Impeding this down-regulation results in increased ROS levels, impaired ATP production and reduced male competence (Cai et al., 2015).

In this study, we identified the endonuclease M20, a plant mitochondrial DNase, providing direct evidence for the molecular participation of DNase in mtDNA down-regulation. The discovery of M20 in the mitochondria does not conflict with the reported function of DPD1, but rather, it helps elucidate the molecular mechanism underlying mtDNA degradation, as the exonuclease DPD1 requires the participation of an endonuclease when degrading circular mtDNA. Our in vitro assay showing the rapid digestion of plasmid DNA by DPD1 in the presence of AtM20 (Fig. 7A) supports this idea. To provide a clearer picture of the roles of AtM20 and DPD1 in regulating mtDNA levels in pollen, we quantified mtDNA in the pollen of *DPD1*-knockout plants. The BCP, early TCP, and late TCP cells possessed  $141.7 \pm 13.6$ ,  $116.7 \pm 8.1$ , and  $106.0 \pm 16.5$  copies of mtDNA (Supplemental Fig. S13), respectively. These results confirm that mtDNA degradation in pollen is impeded in the absence of DPD1, which is in agreement with previous results (Matsushima et al., 2011). Considering that 120 copies of mtDNA are

degraded in Col-0 pollen during pollen development (131.3 [BCP] - 11.3 [late TCP]), Supplemental Figure S8], our analysis suggests that DPD1 may induce approximately 70% ( $[(120 - (141.7 - 106)]/120)$ ) of this degradation, thereby playing a dominant role in mtDNA down-regulation in pollen. Therefore, the remaining 30% of mtDNA degradation might be performed by AtM20 and perhaps other, yet-to-be-identified, DNases. Although the progression of mtDNA degradation was quite slow in *atm20* pollen, late TCP grains had mtDNA levels (17.0 copies/pollen) very close to the minimum appropriate value (11.3 copies in Col-0; Fig. 7B). These results strongly suggest that the endonucleases within pollen mitochondria play redundant roles (Fig. 7C). The identification of M30, with lower in-gel activity than M20 (Fig. 1B), and the slow mtDNA degradation in the absence of AtM20 are in accordance with this suggestion. Thus, completely elucidating the molecular mechanism underlying mtDNA down-regulation would require the characterization of additional endonucleases such as M30.

The aim of this study was to reveal the molecular mechanism underlying mtDNA down-regulation, an important component in maintaining the balance of mtDNA levels in eukaryotic cells. We identified the mitochondrial endonuclease M20, developed a working model for its activity in conjunction with the exonuclease DPD1, and proposed the existence of other endonuclease molecules in mitochondria. The possible molecular redundancy of endonuclease activity highlights the complexity of the mechanism underlying mtDNA down-regulation. We also demonstrated that *AtM20* is extensively transcribed in various tissues of Col-0 plants (Fig. 3B; Supplemental Fig. S3) but that mtDNA levels are not altered in the leaf cells of *AtM20* knockout plants (Supplemental Fig. S11). This finding indicates that the absence of AtM20 has little or no effect on somatic cells, which is in agreement with the absence of other phenotypes in pollen (Fig. 6; Supplemental Fig. S10). Similar phenomena were observed in *DPD1* knockout plants. Although *DPD1* transcript levels are much higher than *AtM20* transcript levels in various tissues (Tang and Sakamoto, 2011), neither vegetative development nor mtDNA levels are abnormal in the somatic cells of *DPD1* knockout plants (Matsushima et al., 2011). The insensitivity of mtDNA to the knockout of mitochondrial DNases adds another level of complexity to our understanding of the regulatory mechanism of mtDNA in the somatic cells of plants. Perhaps this effect is due to the redundancy of DNase activity in somatic mitochondria. Alternatively, a balanced reduction in mtDNA duplication may also help stabilize mtDNA copy number in *DPD1* or *AtM20* knockout plants. Therefore, pollen cells, which exhibit almost complete silencing of mtDNA duplication and protection factor genes (such as genes encoding PolIA, single-stranded DNA binding protein, SSB, and WHIRLY2; from the array data by Honys and Twell, 2004), may serve as an ideal model for further analyzing the down-regulation of mtDNA.

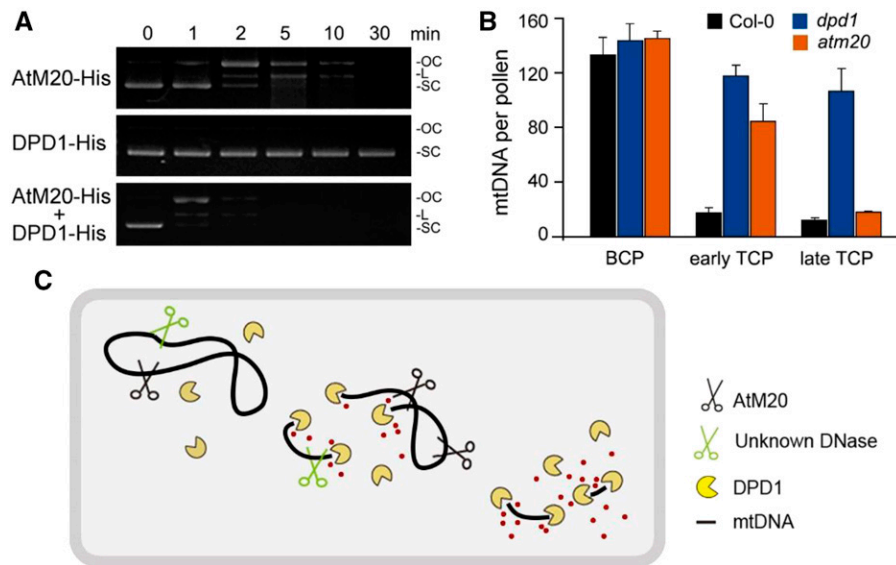


**Figure 7.** Possible role of AtM20 in the down-regulation of mtDNA. A, In vitro assay showing rapid DPD1-induced digestion of circular plasmid DNA in the presence of AtM20. OC, open-circular DNA; L, linear DNA; SC, supercoiled DNA. B, Histogram summarizing mtDNA levels per Col-0, *dpd1*, and *atm20* pollen grain (the results of analyses shown in Supplemental Figs. S8 and S13). Error bars represent the *sd* ( $n = 3$ ). C, Schematic diagram of the degradation of mtDNA by endo- and exonucleases.

## MATERIALS AND METHODS

### Plant Material and Growth Conditions

*Zea mays* pollen was collected from cultivar Zhengdan 951. *Arabidopsis* (*Arabidopsis thaliana*) ecotype Col-0 was used as wild-type plant material for the mutagenesis experiments. *Arabidopsis* seeds were first germinated on 50% Murashige and Skoog medium containing 3% (w/v) Suc and solidified with 0.8% (w/v) agar. The seedlings were transferred into soil and grown in a greenhouse at 22°C with a light/dark cycle of 16 h/8 h.

### Mitochondria Purification from *Zea mays* Pollen

*Zea mays* pollen grains (14,100g) were collected for purification. All procedures were carried out at 4°C. Pollen grains were collected in 1,000 mL of pretreatment buffer (30 mM 3-(N-morpholino)propanesulfonic acid buffer (MOPS) [pH 7.3], 1 mM EDTA, 0.2% [w/v] bovine serum albumin, 30% [w/v] Suc), suspended for 30 min, and transferred into shock buffer (30 mM MOPS [pH 7.3], 1 mM EDTA, 0.2% [w/v] bovine serum albumin, 13% [w/v] Suc) to burst. The mixture was centrifuged for 5 min at 500g. The suspension was collected, filtered through a 20- $\mu$ m pore nylon mesh filter, and centrifuged for 10 min at 4,000g. The supernatant was then centrifuged for 20 min at 11,800g, and the pellet (crude pollen mitochondria) was resuspended with 50 mL wash buffer (30 mM MOPS [pH 7.3], 1 mM EDTA, 13% Suc) and centrifuged for 5 min at 1,000g to separate the nuclear and plastid material. The supernatant was centrifuged for 15 min at 12,000g to precipitate the mitochondria pellet. The pellet was resuspended with 5 mL wash buffer, and the suspension was loaded onto a buffer gradient (90 mM MOPS [pH 7.3], 1 mM EDTA, with Suc content of 20% [10 mL], 40% [6 mL], and 50% [10 mL]) in 50-mL tubes (the gradient buffer was prepared just before use). Next, the samples were ultra-centrifuged for 1 h at 18,000g using a swinging rotor (centrifuge, Optima L8-80XP, Beckman; rotor, SW32Ti). The purified mitochondria were collected within the interface between the 40% and 50% Suc sections. The mitochondria were then diluted twice with wash buffer and centrifuged for 20 min at 21,000g. The pellet was resuspended, frozen in liquid nitrogen, and stored at -80°C.

### Fluorescence and Electron Microscopy

For the fluorescent microscopy experiments, the mitochondria were stained with 500 nM MitoTracker Green FM (Thermo Fisher) for 15 min and

observed under an inverted epifluorescence microscope (Leica DMI6000 B). Photomicrographs were captured with a CCD camera (Leica DFC420) using the Leica Application Suite (V4.2).

For the electron microscopy experiments, purified mitochondria were fixed, embedded, sectioned, and photographed using an electron microscope (JEOL-1010) according to a described protocol (Ma et al., 2017).

### Protein Purification and Identification from Mitochondria

All purification steps were carried out at 4°C, and every chromatography step was carried out using an automatic fast protein liquid chromatography (FPLC) station (Amersham Pharmacia Biotech).

Purified mitochondria were resuspended in mitochondria lysis buffer (100 mM Tris-HCl [pH 8.0], 2% Triton X-100, 15 mM EDTA, 200 mM NaCl, 1 mM phenylmethylsulfonyl fluoride, 0.1%  $\beta$ -mercaptoethanol) and homogenized at 500 rpm for 40 min. The sample was shaken on ice for 20 min and centrifuged for 20 min at 9,000g, after which the supernatant was obtained as total protein sample from the pollen mitochondria.

After obtaining total protein samples from pollen mitochondria, ammonium sulfate was added to reach a final concentration of 1.17 M. After rotating the mixture on ice for 30 min, the sample was centrifuged for 20 min at 11,000g. Ammonium sulfate was added to a final concentration of 1.95 M, and the mixture was stirred for 30 min. The sample was centrifuged for 20 min at 11,000g. The precipitate was resuspended with buffer A (50 mM Tris-HCl [pH 7.5], 0.1% 3-((3-cholamidopropyl) dimethylammonio)-1-propanesulfonate (CHAPS), 200 mM Suc, 1 M ammonium sulfate), rotated for 20 min, and centrifuged for 20 min at 11,000g. The supernatant was applied to a phenyl sepharose 6 Fast Flow column (GE Healthcare). Before running, the column was pre-equilibrated with binding buffer (50 mM Tris-HCl [pH 7.5], 0.1% CHAPS, 200 mM Suc, 1 M ammonium sulfate) at a flow rate of 1 mL/min. After loading the sample on the column, it was eluted in a 50-mL linear gradient of elution buffer (50 mM Tris-HCl [pH 7.5], 0.1% CHAPS, 200 mM Suc) at a flow rate of 1 mL/min. Fractions of 3 mL were collected and numbered, and their nuclease activity was tested. The obtained elution fractions were divided into two parts, which were used in different purification flow paths.

For one part, the sample was dialyzed overnight, concentrated, and loaded on a RESOURCE S IEX column (GE Healthcare) equilibrated with 3 column volumes of binding buffer (50 mM Tris-HCl [pH 7.5], 0.1% CHAPS, 0.1%  $\beta$ -mercaptoethanol) at 5 mL/min. The column was eluted with 20 column volumes of a linear gradient (from 0% to 100%) of elution buffer (50 mM Tris-HCl [pH 7.5], 0.1% CHAPS, 1 M NaCl, 0.1%  $\beta$ -mercaptoethanol) at a flow rate of

1 mL/min. Fractions of 1 mL were collected and numbered, and their nuclease activity was tested. The fractions with the most enzymatic activity were concentrated to 500  $\mu$ L. Each sample was expanded to 1 mL by adding 500  $\mu$ L of loading buffer (5% acetonitrile, 0.1% trifluoroacetic acid) prior to HPLC. For the HPLC analysis, a SunChrom C8 5- $\mu$ m column was used with a linear gradient of acetonitrile in water (0–100% [v/v], over 160 min) containing 0.1% trifluoroacetic acid. The flow rate was maintained at 0.5 mL/min. The area of each product peak was collected, and each peak was identified by LC-MS.

For the other part, the sample was loaded on a Superdex-75 16/60 gel-filtration column. This column was pre-equilibrated with 150 mL of binding buffer (50 mM Tris-HCl [pH 7.5], 0.1% CHAPS, 150 mM NaCl, 0.1%  $\beta$ -mercaptoethanol) at a flow rate of 1 mL/min. The column was eluted with binding buffer at a flow rate of 0.5 mL/h. Fractions were collected and assayed for M20 activity. The active fractions from the gel-filtration column were treated at 100°C for 20 s and centrifuged for 10 min at 17,000g. The samples were subjected to 12.5% SDS-PAGE, after which the positive bands were cut and analyzed by LC-MS.

### LC-MS/MS Protein Identification

The gel bands containing the protein sample were manually excised. Each of the protein bands was digested individually. The protein bands were cut into small plugs and washed twice in 200 mL of distilled water for 10 min. The gel bands were dehydrated in 100% acetonitrile for 10 min and dried in a Speedvac (Labconco) for approximately 15 min. Reduction (10 mM dithiothreitol in 25 mM  $\text{NH}_4\text{HCO}_3$  for 45 min at 56°C) and alkylation (40 mM iodoacetamide in 25 mM  $\text{NH}_4\text{HCO}_3$  for 45 min at room temperature in the dark) were performed, after which the gel plugs were washed twice with 50% acetonitrile in 25 mM ammonium bicarbonate. The gel plugs were then dried using a Speedvac and digested with sequence-grade modified trypsin (40 ng for each band) in 25 mM  $\text{NH}_4\text{HCO}_3$  overnight at 37°C. The enzymatic reaction was stopped by adding formic acid to a 1% final concentration. The solution was then transferred to a sample vial for LC-MS/MS analysis.

LC-MS/MS analysis was performed using a Thermo Fisher Finnigan LTQ linear ion trap mass spectrometer in line with a Thermo Fisher Finnigan Surveyor MS Pump Plus HPLC system. Tryptic peptides generated as described above were loaded onto a trap column (300SB-C18, 5  $\times$  0.3 mm, 5  $\mu$ m particle; Agilent Technologies), which was connected through a zero-dead-volume union to a self-packed analytical column (C18, 100  $\mu$ m 4.6  $\times$  100 mm, 3  $\mu$ m particle; SunChrom). The peptides were then eluted over a gradient (0%–45% B over 55 min, 45%–100% B over 10 min, where B = 80% acetonitrile/0.1% formic acid) at a flow rate of 500 nL/min and introduced online into the linear ion trap mass spectrometer (Thermo Fisher) using nano-electrospray ionization (ESI). Data-dependent scanning was incorporated to select the five most abundant ions (one microscan per spectra, 1.0 *m/z* precursor isolation width, 35% collision energy, 30 ms ion activation, 90 s exclusion duration, repeat count 1) from a full-scan mass spectrum for fragmentation by collision induced dissociation (CID).

The MS data were analyzed using SEQUEST against the *Zea mays* database, and results were filtered, sorted, and displayed using Bioworks 3.2. Peptides with +1, +2, or +3 charge states were accepted if they were fully enzymatic and had a cross correlation (*Xcorr*) of 1.90, >2.5, and >3.0, respectively. The following residue modifications were allowed in the search: carbamidomethylation on Cys and oxidation on Met. The search was made with a peptide tolerance of 3 Amu and a fragment ion tolerance of 1.0 Amu.

### Nuclease Activity Assay

In-gel SDS-PAGE zymography for detection of nuclease activity was performed as previously described (Rosenthal and Lacks, 1977). The reaction buffer (25  $\mu$ L) consisted of 10 mM Tris-HCl, 0.1 mM EDTA (pH 8.5), 5 mM  $\text{MgCl}_2/\text{CaCl}_2/\text{ZnSO}_4/\text{MnSO}_4$ , and 0.1%  $\beta$ -mercaptoethanol.

For the inhibition analyses using purified M20 and the expressed fusion proteins, the reaction buffer (25  $\mu$ L) consisted of 10 mM Tris-HCl, 0.1 mM EDTA (pH 8.5), 5 mM  $\text{MgCl}_2$ , 0.1%  $\beta$ -mercaptoethanol, and DNA substrates (250 ng of pUC18 plasmid or 1  $\mu$ g of salmon sperm DNA). Proteins (2.5  $\mu$ g) were added to initiate the reaction. The reactions were conducted at 37°C and completed by adding stopping buffer (1% [w/v] SDS, 50% [v/v] glycerol, and 0.05% [w/v] bromophenol blue). The reaction products were subjected to 1% (w/v) agarose gel electrophoresis. The gel was visualized by a UV video capture system (HEROS BIO) after staining with ethidium bromide.

### Bioinformatics and Phylogenetic Analysis

We used the NCBI (<http://www.ncbi.nlm.nih.gov/>) and TAIR (<http://www.arabidopsis.org>) databases to analyze the genetic sequences of M20 and AtM20. To generate the phylogenetic tree, the M20 (ACG45136) protein sequence from *Zea mays* was used to perform a BLAST search in NCBI that identified sequences with high similarity. These sequences were imported into ClustalW (gap open penalty, 11; gap extension penalty, 1; BLOSUM62) for alignment. Phylogenetic analysis was conducted using MEGA version 4.0 with the neighbor-joining algorithm. All parameters were set to their default values.

### RNA Extraction and RT-PCR

Total RNA was extracted from maize and Arabidopsis tissue samples using Trizol reagent (Invitrogen) according to the manufacturer's instructions. To synthesize the complementary DNA (cDNA), total RNA was reverse-transcribed using the PrimeScript first Strand cDNA Synthesis Kit (TaKaRa).

### Plasmid Construction

#### Construction for Recombinant Protein Expression and Site-Directed Mutagenesis

The M20 coding sequence (CDS) was PCR amplified with M20\_F and M20\_R primers (all primers are listed in Supplemental Table S2) from maize cDNA. The fragment was cloned into the *Bam*HI and *Not*I sites of pGEX-4T-1 to generate the pGEX-M20 vector. pET28a-AtM20 was constructed by amplifying the AtM20 CDS with AtM20\_F and AtM20\_R from Arabidopsis Col-0 cDNA, and the fragment was cloned into the *Nco*I and *Hind*III sites of the pET28a plasmid.

To perform site-directed mutation of M20 and AtM20, PCR-based site-directed mutagenesis was performed with primers (M20\_m1 and M20\_m2 for M20; AtM20\_m1 and AtM20\_m2 for AtM20) using the QuickChange Multi Site-Directed Mutagenesis Kit (Stratagene) according to the instruction manual. The altered fragments (H82D, N96A, or N105A for M20; H92D, N106A, or N115A for AtM20) were sequenced and subcloned into pBI121-35S<sub>pro</sub>-GFP to generate three pBI121-35S<sub>pro</sub>- $\Delta$ M20(H82D/N96A/N105A)-GFP plasmids and 35S<sub>pro</sub>- $\Delta$ AtM20(H92D/N106A/N115A)-GFP plasmids, respectively. pBI121-35S<sub>pro</sub>-GFP was constructed by modifying pBI121-JGB<sub>pro</sub>-GFP (Ju et al., 2016) by replacing the JGB promoter with the CaMV 35S promoter. Finally, the  $\Delta$ M20-GFP and  $\Delta$ AtM20-GFP fragments were each cloned into the pET28a plasmid.

#### Construction for Spatiotemporal Expression Analysis

To construct pBI121-AtM20<sub>pro</sub>-GUS, a 1,718-bp fragment upstream of the start codon of AtM20 (termed the AtM20 promoter) was amplified with AtM20pro\_F and AtM20pro\_R from Col-0 genomic DNA and cloned into the *Hind*III and *Sma*I sites of the pBI121 vector.

For the subcellular localization assay, three constructs were made: pGreen-35S<sub>pro</sub>-AtM20-GFP and pGreen-35S<sub>pro</sub>-GFP for transient expression in *Nicotiana benthamiana* leaf cells and pBI121-AtM20<sub>pro</sub>-AtM20-GFP for stable transformation of Arabidopsis. To construct pGreen-35S<sub>pro</sub>-GFP, the 35S promoter was amplified with the *Xho*I-35S\_F and 35S-*Hind*III\_R primers, and GFP was amplified with *Hind*III-GFP\_F and GFP-*Eco*RI\_R. These two fragments were cloned into the *Xho*I and *Eco*RI sites of the pGreen0179 plasmid. To construct pGreen-35S<sub>pro</sub>-AtM20-GFP, the AtM20 CDS (without a stop codon) was amplified with the *Hind*III-AtM20\_F and AtM20-G5-*Eco*RI\_R primers from Arabidopsis Col-0 cDNA and cloned into the *Hind*III and *Eco*RI sites of the pGreen0179 plasmid. Next, the MCS fragment between *Eco*RI and *Xba*I was replaced with the GFP fragment.

To construct pBI121-AtM20<sub>pro</sub>-AtM20-GFP, the AtM20 promoter was amplified with *Kpn*I-AtM20Pro\_F and AtM20Pro-*Xho*I\_R from Col-0 genomic DNA, and the AtM20 CDS (without a stop codon) was amplified with *Xho*I-AtM20\_F and AtM20-SpeI\_R from Col-0 cDNA. These two fragments were ligated into the *Kpn*I and *Spe*I sites of the pBI121-JGB<sub>pro</sub>-JGB-GFP vector (Ju et al., 2016).

#### Construction for Genetic Complementation

The pBI121-AtM20<sub>pro</sub>-AtM20 vector was constructed by ligating the AtM20 promoter fragment and AtM20 CDS fragment into the pBI121 vector between

the *KpnI* and *SacI* sites. The *AtM20* promoter was amplified with the *KpnI*-*AtM20Pro\_F* and *AtM20Pro-XhoI\_R* primers from Col-0 genomic DNA, and the *AtM20* CDS was amplified with *XhoI*-*AtM20\_F* and *AtM20-SacI\_R* from Col-0 cDNA.

## Transient and Stable Genetic Transformation

Plasmids were introduced into *Agrobacterium tumefaciens*. For transient transformation, the transformants were used to infiltrate *Nicotiana benthamiana* leaves as described previously (Waadt and Kudla, 2008). After 48 h, the infiltrated leaves were enzymolyzed with enzymolysis buffer (0.1% [w/v] pectinase Y-23, 1% [w/v] cellulose-RS, 0.4 M mannitol, 20 mM 2-(N-morpholino)ethanesulfonic acid (MES) [pH 5.5], 100 mM MitoTracker Red CMXRos, Thermo Fisher) and subjected to observation using a confocal microscope (Olympus FV3000). For stable genetic transformation, plants were treated with *Agrobacterium tumefaciens* strain GV3101 via the floral-dipping method (Clough and Bent, 1998).

## Recombinant Protein Expression

Constructed vectors were transformed into *Escherichia coli* strain BL21 (TransGen Biotech). Protein induction expression was performed with 1 mM isopropyl  $\beta$ -D-1-thiogalactopyranoside in 400 mL of culture medium. M20-GST and *AtM20*-His were purified using glutathione sepharose 4 B and ni sepharose 6 Fast Flow (GE Healthcare), respectively, according to the manufacturer's instructions.

## Expression Pattern Analysis

Histochemical staining for GUS activity was performed using a previously described method (Ju et al., 2016). RT-qPCR was used to determine the spatial expression pattern of *AtM20*. Total RNA was extracted from different tissues (root, stem, leaf, flower, and pollen grains) from Col-0 plants as described above. A 561-bp fragment of *AtM20* was amplified with primer pair *AtM20RT\_F* and *AtM20RT\_R* to evaluate the expression level of *AtM20* in different tissues and at different stages. The housekeeping gene histone H3 (*At4g40040*) was used for normalization (primers *H3\_F* and *H3\_R*). The PCR products were checked by 1.5% agarose gel electrophoresis.

## Mutant Verification

All T-DNA insertion alleles in *AtM20* were obtained from the ABRC (CS825515, SALK-084907, SALK-113210, SALK-140217, and SALK-140219) and the GABI-Kat (934A04) seeds center. Total genomic DNA was isolated by a cetyl-trimethyl-ammonium bromide protocol (Murray and Thompson, 1980). Gene-specific primers (see Supplemental Table S2), together with the *Lba1/TP* primer (<http://signal.salk.edu/tdnaprimers.2.html>), were used to test the T-DNA insertion lines.

## Generation of *atm20* Mutants Using CRISPR-Cas9 Technology

For each *AtM20* targeting site, two complementary 24-bp oligonucleotides with a 20-bp target sequence were synthesized (sequences of the synthesized DNA oligos are shown in Supplemental Table S2). The oligo pairs were annealed to generate three double-stranded DNAs with 4-bp overhangs on both ends and cloned into the *BbsI* sites of the *AtU6-26SK* vector (Feng et al., 2013). Next, the three chimeric sgRNA cassettes between *KpnI* and *SallI* in *AtU6-26SK* were cloned into the *KpnI* and *EcoRI* region of the pCambia1300 vector, together with the *SallI* and *EcoRI* fragment of the hSpCas9 expression cassette from 35S<sub>pro</sub>-Cas9-SK (Feng et al., 2013). The constructed pCambia1300 vectors were introduced into *Agrobacterium* strain GV3101. Arabidopsis Col-0 wild-type plants were stably transformed via the floral-dipping method (Clough and Bent, 1998). Transformants were screened on 1/2 Murashige and Skoog plates with 40  $\mu$ g/L hygromycin. The genomic DNA of wild-type and stable transgenic plants was extracted and used as a template for PCR with specific primers (Supplemental Table S2) for each site. The PCR products were analyzed by Sanger sequencing.

## Fluorescence Microscopy

To allow direct observation of the mtDNA signal from vegetative pollen cells, fresh pollen grains were immersed in staining buffer (20 mM Tris-HCl

[pH 7.7], 0.5 mM EDTA, 1.2 mM spermidine, 7 mM 2-mercaptoethanol) (Nemoto et al., 1988) supplemented with 10  $\mu$ g/mL 4',6-diamino-phenylindole (Invitrogen) on a glass slide and crushed by the described method (Matsushima et al., 2011). The samples were examined with an epifluorescence microscope (DMI 6000B; Leica) and captured with a CCD camera (DFC480; Leica).

## Determination of mtDNA Copy Number

The relative mtDNA levels in the total DNA samples were measured by amplification of the mitochondrial *cox1* gene (*psbA* gene for plastid DNA quantification) and nuclear *18S* rRNA gene with specific primers (Supplemental Table S2; Rowan et al., 2009). Total DNA samples were prepared from pollen cells and young seedlings. Amplification was conducted using a LightCycler II Real-Time PCR System (Roche) with SYBR premix ExTaq (TaKaRa). qPCR was performed in a 10- $\mu$ L reaction mixture containing 5  $\mu$ L of SYBR premix ExTaq, 0.2 mM of each primer, and 40 ng of genomic DNA. The amplification procedure was 95°C for 10 min followed by 45 cycles of 95°C for 20 s and 60°C for 45 s. The data were analyzed using LightCycler3 software (Roche). The abundance of mtDNA was normalized to that of *18S* rRNA using the  $\Delta C_T$  method (Livak and Schmittgen, 2001).

To further evaluate the mtDNA level in *atm20* and Col-0 pollen, extracts from five pollen grains were subjected to PCR. The *nad9* gene was amplified (Matsushima et al., 2011), and the products were subjected to 1.5% (w/v) agarose gel electrophoresis. After staining with ethidium bromide, the gels were imaged and quantified using software (ImageJ; NIH).

Absolute quantification of mtDNA copy number in single pollen cells was conducted by a competitive PCR method described by Wang et al. (2010). In brief, five pollen grains for each quantification were crushed and pretreated by rapid freezing, thawing, and proteinase K digestion. The resulting mixture was divided into five aliquots. The mtDNA copy number per pollen grain was obtained after two rounds of competitive PCR with mitochondrial *matR* as the target.

## Analysis of Pollen Viability and Pollen Germination

For the pollen viability test, pollen grains were collected from stage 13 Arabidopsis flowers and stained with Alexander stain for 2 h (Alexander, 1969). For in vitro germination, mature pollen grains from newly opened flowers were collected and placed onto the germination medium (0.01% [w/v]  $H_3BO_3$ , 5 mM KCl, 5 mM  $CaCl_2$ , 1 mM  $MgSO_4$ , and 18% [w/v] Suc, pH 7.5; 1.5% [w/v] agar; Boavida and McCormick, 2007). To detect the pollen tube elongation efficiency, the pre-emasculated wild-type stigmas were pollinated with 40 to 60 pollen grains. After specific periods of tube growth, the stigmas were fixed in acetic acid/ethanol (v:v = 1:3) solution, cleared in 8 M NaOH, and stained with Aniline Blue (Mori et al., 2006). The images of germinated pollen and pollen tubes stained by Aniline Blue in the pistils were captured with a CCD camera (DFC480; Leica) using a microscope (DMI 6000B; Leica).

## Accession Numbers

Sequence data from this article can be found in the Arabidopsis Genome Initiative or GenBank/EMBL databases under the following accession numbers: *Zea mays* M20, ACG45126; *Arabidopsis thaliana* *AtM20*, At1g18680; *Arabidopsis thaliana* *DPD1*, At5g26940; *Oryza sativa* *Japonica*, XP\_015613125.1; *Picea sitchensis*, ABK21604; *Sorghum bicolor*, XP\_002467035.1; *Vitis vinifera*, XP\_003634305.1; *Selaginella moellendoffii*, XP\_002992844.1; *Physcomitrella patens*, XP\_001755719.1.

## Supplemental Data

The following supplemental materials are available.

**Supplemental Figure S1.** Isolation of maize pollen mitochondria and purification of M20.

**Supplemental Figure S2.** Sequence alignment and phylogenetic analysis of M20.

**Supplemental Figure S3.** Tissue-specific expression pattern of *AtM20* predicted using the Arabidopsis eFP Browser database.

- Supplemental Figure S4.** AtM20 levels are elevated in pollen mitochondria.
- Supplemental Figure S5.** Transcriptional analysis of *AtM20* T-DNA insertion mutants.
- Supplemental Figure S6.** Mutation of *AtM20* via CRISPR/Cas9.
- Supplemental Figure S7.** Preservation of fluorescent signals from organelle DNA in the early TCPs of three additional independent T1 CRISPR/Cas9 mutant lines.
- Supplemental Figure S8.** Quantification of mtDNA per pollen grain using the single-cell-based competitive PCR method.
- Supplemental Figure S9.** Introducing the *AtM20* coding sequence into the *atm20* mutant rescues the impeded mtDNA degradation in the mutant.
- Supplemental Figure S10.** Plant architecture and reproductive ability of *atm20* homozygous mutants.
- Supplemental Figure S11.** Organelle DNA in mesophyll cells.
- Supplemental Figure S12.** Degradation of plastid DNA in pollen vegetative cells is not affected in the *atm20* mutant.
- Supplemental Figure S13.** Copy number of mtDNA per single *dpd1* pollen grain quantified using the competitive PCR method.
- Supplemental Table S1.** Segregation analysis via reciprocal crosses between Col-0 and heterozygous *atm20* plants.
- Supplemental Table S2.** Primers (DNA oligos) used in this study.

## ACKNOWLEDGMENTS

We thank Wataru Sakamoto for generously providing the transgenic Arabidopsis seed (LAT52pro-Dips-RFP) and vectors (pGreen0029-DUO1-DIPS-GFP-NOS); Jian-Kang Zhu for providing the Cas9-related plasmids.

Received August 27, 2018; accepted September 21, 2018; published October 9, 2018.

## LITERATURE CITED

- Alam TI, Kanki T, Muta T, Ukaji K, Abe Y, Nakayama H, Takio K, Hamasaki N, Kang D (2003) Human mitochondrial DNA is packaged with TFAM. *Nucleic Acids Res* **31**: 1640–1645
- Alexander MP (1969) Differential staining of aborted and nonaborted pollen. *Stain Technol* **44**: 117–122
- Arimura SI (2018) Fission and fusion of plant mitochondria, and genome maintenance. *Plant Physiol* **176**: 152–161
- Arimura S, Yamamoto J, Aida GP, Nakazono M, Tsutsumi N (2004) Frequent fusion and fission of plant mitochondria with unequal nucleoid distribution. *Proc Natl Acad Sci USA* **101**: 7805–7808
- Attardi G, Schatz G (1988) Biogenesis of mitochondria. *Annu Rev Cell Biol* **4**: 289–333
- Boavida LC, McCormick S (2007) Temperature as a determinant factor for increased and reproducible in vitro pollen germination in *Arabidopsis thaliana*. *Plant J* **52**: 570–582
- Bogenhagen D, Clayton DA (1977) Mouse L cell mitochondrial DNA molecules are selected randomly for replication throughout the cell cycle. *Cell* **11**: 719–727
- Cai Q, Guo L, Shen ZR, Wang DY, Zhang Q, Sodmergen (2015) Elevation of pollen mitochondrial DNA copy number by WHIRLY2: Altered respiration and pollen tube growth in Arabidopsis. *Plant Physiol* **169**: 660–673
- Canetti L, Lomaniec E, Elkind Y, Lers A (2002) Nuclease activities associated with dark-induced and natural leaf senescence in parsley. *Plant Sci* **163**: 873–880
- Chen HM, Pang Y, Zeng J, Ding Q, Yin SY, Liu C, Lu MZ, Cui KM, He XQ (2012) The Ca<sup>2+</sup>-dependent DNases are involved in secondary xylem development in *Eucommia ulmoides*. *J Integr Plant Biol* **54**: 456–470
- Clay Montier LL, Deng JJ, Bai Y (2009) Number matters: Control of mammalian mitochondrial DNA copy number. *J Genet Genomics* **36**: 125–131
- Clough SJ, Bent AF (1998) Floral dip: A simplified method for *Agrobacterium*-mediated transformation of *Arabidopsis thaliana*. *Plant J* **16**: 735–743
- Dai H, Lo YS, Litvinchuk A, Wang YT, Jane WN, Hsiao LJ, Chiang KS (2005) Structural and functional characterizations of mung bean mitochondrial nucleoids. *Nucleic Acids Res* **33**: 4725–4739
- Dimauro S, Davidzon G (2005) Mitochondrial DNA and disease. *Ann Med* **37**: 222–232
- Emanuelsson O, Nielsen H, Brunak S, von Heijne G (2000) Predicting subcellular localization of proteins based on their N-terminal amino acid sequence. *J Mol Biol* **300**: 1005–1016
- Feng Z, Zhang B, Ding W, Liu X, Yang DL, Wei P, Cao F, Zhu S, Zhang F, Mao Y (2013) Efficient genome editing in plants using a CRISPR/Cas system. *Cell Res* **23**: 1229–1232
- Feng Z, Mao Y, Xu N, Zhang B, Wei P, Yang DL, Wang Z, Zhang Z, Zheng R, Yang L (2014) Multigeneration analysis reveals the inheritance, specificity, and patterns of CRISPR/Cas-induced gene modifications in Arabidopsis. *Proc Natl Acad Sci USA* **111**: 4632–4637
- Gross NJ, Getz GS, Rabinowitz M (1969) Apparent turnover of mitochondrial deoxyribonucleic acid and mitochondrial phospholipids in the tissues of the rat. *J Biol Chem* **244**: 1552–1562
- Gu HT, Wang DH, Li X, He CX, Xu ZH, Bai SN (2011) Characterization of an ethylene-inducible, calcium-dependent nuclease that is differentially expressed in cucumber flower development. *New Phytol* **192**: 590–600
- Higuchi M (2007) Regulation of mitochondrial DNA content and cancer. *Mitochondrion* **7**: 53–57
- Hony D, Twell D (2004) Transcriptome analysis of haploid male gametophyte development in Arabidopsis. *Genome Biol* **5**: R85
- Ju Y, Guo L, Cai Q, Ma F, Zhu QY, Zhang Q, Sodmergen S (2016) Arabidopsis JINGUBANG is a negative regulator of pollen germination that prevents pollination in moist environments. *Plant Cell* **28**: 2131–2146
- Kai Y, Takamatsu C, Tokuda K, Okamoto M, Irita K, Takahashi S (2006) Rapid and random turnover of mitochondrial DNA in rat hepatocytes of primary culture. *Mitochondrion* **6**: 299–304
- Kayal E, Bentlage B, Collins AG, Kayal M, Pirro S, Lavrov DV (2012) Evolution of linear mitochondrial genomes in *medusozoan cnidarians*. *Genome Biol Evol* **4**: 1–12
- Klein M, Eckert-Ossenkopp U, Schmiedebert I, Brandt P, Unseld M, Brennicke A, Schuster W (1994) Physical mapping of the mitochondrial genome of *Arabidopsis thaliana* by cosmid and YAC clones. *Plant J* **6**: 447–455
- Kolodner R, Tewari KK (1972) Physicochemical characterization of mitochondrial DNA from pea leaves. *Proc Natl Acad Sci USA* **69**: 1830–1834
- Kool AJ, de Haas JM, Mol JN, van Marrewijk GA (1985) Isolation and physicochemical characterization of mitochondrial DNA from cultured cells of *Petunia hybrida*. *Theor Appl Genet* **69**: 223–233
- Liu B, Wang J, Yildirim G, Englund PT (2009) TbPIF5 is a *Trypanosoma brucei* mitochondrial DNA helicase involved in processing of minicircle Okazaki fragments. *PLoS Pathog* **5**: e1000589
- Livak KJ, Schmittgen TD (2001) Analysis of relative gene expression data using real-time quantitative PCR and the 2<sup>−(ΔΔC(T))</sup> method. *Methods* **25**: 402–408
- Lombardi L, Ceccarelli N, Picciarelli P, Lorenzi R (2007) DNA degradation during programmed cell death in *Phaseolus coccineus* suspensor. *Plant Physiol Biochem* **45**: 221–227
- Luo D, Xu H, Liu Z, Guo J, Li H, Chen L, Fang C, Zhang Q, Bai M, Yao N (2013) A detrimental mitochondrial-nuclear interaction causes cytoplasmic male sterility in rice. *Nat Genet* **45**: 573–577
- Ma F, Hu Y, Ju Y, Jiang Q, Cheng Z, Zhang Q, Sodmergen (2017) A novel tetratricopeptide repeat protein, WHITE TO GREEN1, is required for early chloroplast development and affects RNA editing in chloroplasts. *J Exp Bot* **68**: 5829–5843
- Magnusson J, Orth M, Lestienne P, Taanman JW (2003) Replication of mitochondrial DNA occurs throughout the mitochondria of cultured human cells. *Exp Cell Res* **289**: 133–142
- Maier D, Farr CL, Poeck B, Alahari A, Vogel M, Fischer S, Kaguni LS, Schneuwly S (2001) Mitochondrial single-stranded DNA-binding protein is required for mitochondrial DNA replication and development in *Drosophila melanogaster*. *Mol Biol Cell* **12**: 821–830
- Masuyama M, Iida R, Takatsuka H, Yasuda T, Matsuki T (2005) Quantitative change in mitochondrial DNA content in various mouse tissues during aging. *Biochim Biophys Acta* **1723**: 302–308
- Matsushima R, Tang LY, Zhang L, Yamada H, Twell D, Sakamoto W (2011) A conserved, Mg<sup>2+</sup>-dependent exonuclease degrades organelle DNA during Arabidopsis pollen development. *Plant Cell* **23**: 1608–1624

- Mehta P, Katta K, Krishnaswamy S** (2004) HNH family subclassification leads to identification of commonality in the His-Me endonuclease superfamily. *Protein Sci* **13**: 295–300
- Miao J, Guo D, Zhang J, Huang Q, Qin G, Zhang X, Wan J, Gu H, Qu LJ** (2013) Targeted mutagenesis in rice using CRISPR-Cas system. *Cell Res* **23**: 1233–1236
- Mittler R, Lam E** (1995) Identification, characterization, and purification of a tobacco endonuclease activity induced upon hypersensitive response cell death. *Plant Cell* **7**: 1951–1962
- Mori T, Kuroiwa H, Higashiyama T, Kuroiwa T** (2006) GENERATIVE CELL SPECIFIC 1 is essential for angiosperm fertilization. *Nat Cell Biol* **8**: 64–71
- Murray MG, Thompson WF** (1980) Rapid isolation of high molecular weight plant DNA. *Nucleic Acids Res* **8**: 4321–4325
- Nagata N, Saito C, Sakai A, Kuroiwa H, Kuroiwa T** (1999) The selective increase or decrease of organellar DNA in generative cells just after pollen mitosis one controls cytoplasmic inheritance. *Planta* **209**: 53–65
- Nair R, Rost B** (2005) Mimicking cellular sorting improves prediction of sub-cellular localization. *J Mol Biol* **348**: 85–100
- Nemoto Y, Kawano S, Nakamura S, Mita T, Nagata T, Kuroiwa T** (1988) Studies on plastid-nuclei (nucleoids) in *Nicotiana tabacum* L. 1. Isolation of proplastid-nuclei from cultured-cells and identification of proplastid-nuclear proteins. *Plant Cell Physiol* **29**: 167–177
- Parent JS, Lepage E, Brisson N** (2011) Divergent roles for the two Poll-like organelle DNA polymerases of Arabidopsis. *Plant Physiol* **156**: 254–262
- Preuten T, Cincu E, Fuchs J, Zoschke R, Liere K, Börner T** (2010) Fewer genes than organelles: extremely low and variable gene copy numbers in mitochondria of somatic plant cells. *Plant J* **64**: 948–959
- Robin ED, Wong R** (1988) Mitochondrial DNA molecules and virtual number of mitochondria per cell in mammalian cells. *J Cell Physiol* **136**: 507–513
- Rosenthal AL, Lacks SA** (1977) Nuclease detection in SDS-polyacrylamide gel electrophoresis. *Anal Biochem* **80**: 76–90
- Rowan BA, Oldenburg DJ, Bendich AJ** (2009) A multiple-method approach reveals a declining amount of chloroplast DNA during development in Arabidopsis. *BMC Plant Biol* **9**: 3
- Sakamoto W, Takami T** (2014) Nucleases in higher plants and their possible involvement in DNA degradation during leaf senescence. *J Exp Bot* **65**: 3835–3843
- Sakamoto W, Takami T** (2018) Chloroplast DNA dynamics: Copy number, quality control and degradation. *Plant Cell Physiol* **59**: 1120–1127
- Satoh M, Nemoto Y, Kawano S, Nagata T, Hirokawa H, Kuroiwa T** (1993) Organization of heterogeneous mitochondrial-DNA molecules in mitochondrial nuclei of cultured tobacco cells. *Protoplasma* **175**: 112–120
- Schapiro AH** (2012) Mitochondrial diseases. *Lancet* **379**: 1825–1834
- Sharief FS, Vojta PJ, Ropp PA, Copeland WC** (1999) Cloning and chromosomal mapping of the human DNA polymerase  $\theta$  (*POLQ*), the eighth human DNA polymerase. *Genomics* **59**: 90–96
- Sheahan MB, McCurdy DW, Rose RJ** (2005) Mitochondria as a connected population: ensuring continuity of the mitochondrial genome during plant cell dedifferentiation through massive mitochondrial fusion. *Plant J* **44**: 744–755
- Shen J, Zhao J, Bartoszewski G, Malepszy S, Havey M, Chen J** (2015) Persistence and protection of mitochondrial DNA in the generative cell of cucumber is consistent with its paternal transmission. *Plant Cell Physiol* **56**: 2271–2282
- Sodmergen, Suzuki, T., Kawano, S., Nakamura, S., Tano, S., and Kuroiwa, T.** (1992) Behavior of organelle nuclei (nucleoids) in generative and vegetative cells during maturation of pollen in *Lilium longiflorum* and *Pelargonium zonale*. *Protoplasma* **168**: 73–82
- Sodmergen, Kawano, S., Tano, S., and Kuroiwa, T.** (1991) Degradation of chloroplast DNA in second leaves of rice (*Oryza sativa*) before leaf yellowing. *Protoplasma* **160**: 89–98
- Tang LY, Sakamoto W** (2011) Tissue-specific organelle DNA degradation mediated by DPD1 exonuclease. *Plant Signal Behav* **6**: 1391–1393
- Waadt, R., and Kudla, J.** (2008). In planta visualization of protein interactions using bimolecular fluorescence complementation (BiFC). *CSH Protoc.* 2008: pdb.prot4995.
- Wallace DC** (2008) Mitochondria as chi. *Genetics* **179**: 727–735
- Wallace DC, Murdock DG** (1999) Mitochondria and dystonia: The movement disorder connection? *Proc Natl Acad Sci USA* **96**: 1817–1819
- Wang DY, Zhang Q, Liu Y, Lin ZF, Zhang SX, Sun MX, Sodmergen** (2010) The levels of male gametic mitochondrial DNA are highly regulated in angiosperms with regard to mitochondrial inheritance. *Plant Cell* **22**: 2402–2416
- Wang Z, Zou Y, Li X, Zhang Q, Chen L, Wu H, Su D, Chen Y, Guo J, Luo D,** (2006) Cytoplasmic male sterility of rice with boro II cytoplasm is caused by a cytotoxic peptide and is restored by two related PPR motif genes via distinct modes of mRNA silencing. *Plant Cell* **18**: 676–687
- Wanrooij S, Fusté JM, Farge G, Shi Y, Gustafsson CM, Falkenberg M** (2008) Human mitochondrial RNA polymerase primes lagging-strand DNA synthesis in vitro. *Proc Natl Acad Sci USA* **105**: 11122–11127
- Xie YM, Jin L, Chen XJ, He MN, Wang Y, Liu R, Li MZ, Li XW** (2015) Quantitative changes in mitochondrial DNA copy number in various tissues of pigs during growth. *Genet Mol Res* **14**: 1662–1670